Cross-Strand Pairing and Amyloid Assembly

Yan Liang,[‡] Sai Venkatesh Pingali,[§] Ashutosh S. Jogalekar,[‡] James P. Snyder,*[,‡] Pappannan Thiyagarajan,*[,§] and David G. Lynn*[,‡]

Center for Fundamental and Applied Molecular Evolution, Departments of Chemistry and Biology, Emory University, Atlanta, Georgia 30322, and Advance Photon Source, Argonne National Laboratory, Argonne, Illinois 60439

Received June 8, 2008; Revised Manuscript Received July 28, 2008

ABSTRACT: Amino acid cross-strand pairing interactions along a β-sheet surface have been implicated in protein β-structural assembly and stability, yet the relative contributions have been difficult to evaluate directly. Here we develop the central core sequence of the Aβ peptide associated with Alzheimer's disease, Aβ(16−22), as an experimental system for evaluating these interactions. The peptide allows for internal comparisons between electrostatic and steric interactions within the β-sheet and an evaluation of these cross-strand pair contributions to β-sheet registry. A morphological transition from fibers to hollow nanotubes arises from changes in β-sheet surface complementarity and provides a convenient indicator of the β-strand strand registry. The intrinsic β-sequence and pair correlations are critical to regulate secondary assembly. These studies provide evidence for a critical desolvation step that is not present in most models of the nucleation-dependent pathway for amyloid assembly.

The α- and β-secondary protein structure elements each contribute significantly, but very differently, to polymer folding and stability. In contrast to α-structures where the relative contributions of individual amino acid propensities within the helix can be estimated (*1*−*6*), the longer range tertiary interactions that contribute significantly to β-sheet stability remain difficult to predict (*7*−*10*). An initial survey of 253 known globular protein structures from the Brookhaven Protein Data Bank found that pairwise distributions of amino acids in antiparallel β-sheets are not random (*11*). When viewed along two antiparallel strands (Scheme 1), the amino acid backbone atoms can be either directly hydrogen bonded (H-bonded site) or not bonded (non-H-bonded site), and such cross-strand pairing interactions, which could be stabilizing or destabilizing (*12, 13*), appear to contribute significantly to β-sheet structure.

Recent studies from Koide et al. have featured an in-depth analysis of the outer surface protein A (OspA) from *Borrelia burgdorferi*, a protein that contains a single sheet connecting two globular domains (*14*−*16*). A series of mutants generated by alanine scanning did not correlate with experimental β-sheet propensity scales, statistical β-sheet propensity scales, or cross-strand pairwise interactions (*14*). Instead, the free energy of the assembly of this single β-sheet solvated on both surfaces was most strongly correlated with the buried nonpolar surface area of the assembly. This difference in the energetic factors that contribute most to the assembly of isolated β-sheets and those within globular proteins may well be relevant to the early steps in amyloid assembly and β-sheet nucleation.

Amyloid can be an all-β-peptide assembly and is implicated in more than four dozen disorders including Alzheimer's, Huntington's, and the prion diseases. These fibrous aggregates, which assemble through nucleation-dependent kinetics (*17*−*19*), form a characteristic cross-β spine where peptide strands are arrayed perpendicular to the long fiber axis (*20*−*22*). The resulting three-dimensional arrangement produces characteristic orthogonal X-ray diffraction reflections at ∼5 and ∼10 Å, generally assigned to the spacing between individual strands within a β-sheet and the packing of neighboring sheets as laminates. Although amyloid may well be accessible to all α-amino acid polypeptides (*23*−*25*), surprisingly little is known about the growth mechanism or the molecular structure of the species responsible for disease etiology (*23*). Current models suggest the β assembly of amyloid originates from simple sheets as early nucleation events (*26*−*30*), and this early structure is propagated to create the final assembly.

The seven-residue peptide that constitutes the central core of the Aβ peptide of Alzheimer's disease, Ac-KLVFFAE-NH_2 or Aβ(16−22),[1] presents several valuable and simplifying elements helpful in exploring amyloid assembly. First, Aβ(16−22) is one of the smallest peptides able to form amyloid, and unlike most amyloid fibers, the assemblies of Aβ(16−22) are soluble and readily analyzed spectroscopically. Second, a simple change in strand registry (Scheme 1) is amplified by a switch from amyloid fibers to nanotube morphologies (*31, 32*). And finally, Aβ(16−22) contains complementary charged residues at each terminus and a single β-branched residue at V18. We now report the development of experimental and computational models of

* To whom correspondence should be addressed. Phone: 404-727-9348. Fax: 404-727-6586. E-mail: dlynn2@emory.edu, thiyaga@anl.gov, jsnyder@emory.edu.

[‡] Emory University.

[§] Argonne National Laboratory.

[1] Abbreviations: Aβ(16−22), amyloid β 16−22; dpi, dots per inch; FMOC, 9-fluorenylmethyl chloroformate; IE-FTIR, isotope-edited Fourier transform infrared; SAXS, small-angle X-ray scattering; TDC, transition dipolar coupling; TEM, transmission electron microscopy; TFA, trifluoroacetic acid; WAXS, wide-angle X-ray scattering.

10.1021/bi801081c CCC: $40.75
Published on Web 08/30/2008

Scheme 1: One Residue Shift in a Three-Strand Antiparallel β-Sheet

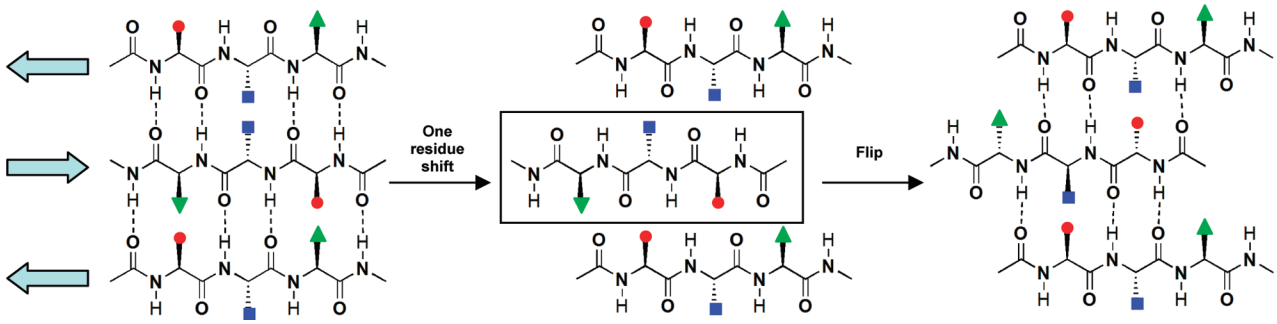

Aβ(16−22) to evaluate contributions to β-sheet assembly in this simple model peptide. We provide evidence that cross-strand pairwise interactions contribute significantly to Aβ(16−22) assembly and that there must exist steps early in the process prior to β-sheet assembly that facilitate peptide desolvation. These results reveal the subtle differences that may regulate morphologically important misfolding assemblies in disease (*32*) and bring into focus the specific early steps of the nucleation-dependent mechanism for their assembly.

MATERIALS AND METHODS

Peptide Synthesis and Purification. Aβ(16−22) and its V18 congeners were synthesized using standard FMOC peptide synthesis protocols on an Applied Biosystems ABI431 peptide synthesizer. The resulting peptides were cleaved from the resin using a solution of TFA/thioanisole/ehtanedithiol/anisole (90/5/3/2 v/v), precipitated from the cleavage solution using excess ice-cold diethyl ether, and washed repeatedly with ice-cold diethyl ether. Reverse-phase HPLC (Water Delta 600) with a linear gradient of acetonitrile and water (0.1% TFA) was used for peptide purification. The molecular weight of each peptide was verified by MALDI mass spectroscopy. Peptides containing F19 1-^{13}C labels were synthesized as described using [1-^{13}C]phenylalanine and also confirmed by MALDI mass spectroscopy.

Nanotube and Fiber Assembly. The nanotubes and fibers were prepared under two conditions in an attempt to exploit the protonation states of the terminal Lys and Glu side chains. Under the first "acidic" condition, purified Aβ(16−22) and its V18 congeners were dissolved respectively in 40% acetonitrile/water with 0.1% TFA to a final concentration of 2.0 mM. The peptide solution was allowed to self-assemble and mature at room temperature for 2 weeks. Under the second "neutral" conditions, purified Aβ(16−22) and its V18 congeners were dissolved respectively in 40% acetonitrile/water to a final concentration of 2.0 mM. Because peptides are purified in an acetonitrile/water gradient containing 0.1% TFA, a solution of 0.1 M NaOH in 40% acetonitrile/water solution was added to give a 0.1 mM NaOH final concentration, and peptide assembly was allowed to mature at room temperature for 2 weeks.

Transmission Electron Microscopy (TEM). Aliquots (20 μL) of a 2 mM solution of Aβ(16−22) or the structural congeners were applied to TEM grids (Formvar/carbon film coated 200 mesh; Electron Microscopy Sciences, Hatfield, PA) and allowed to adsorb for 1 min. Excess peptide solution was wicked off with filter paper before 10 μL of 5% uranyl acetate (Sigma-Aldrich) was added for 3 min to stain the sample. Again, excess fluid was wicked off with filter paper, and the grid was dried under house vacuum overnight. Each micrograph was recorded on a Hitachi H-7500 transmission electron microscope instrument with a tungsten emission filament at an accelerating voltage of 75 kV. Negatives were scanned at 1800 dpi on a Microtek ArtixScan 1800f scanner (Microtek Laboratory, Inc., Carson, CA).

Small Angle X-ray Scattering (SAXS). SAXS was carried out at Sector 12-ID with the Advanced Photon Source (APS) at Argonne National Laboratory using 12 keV X-rays and a Mar CCD with a sample-to-detector distance of 2 m. To reduce radiation damage, the sample solutions were allowed to flow through a 1.5 mm quartz capillary using a Hamilton syringe pump. SAXS intensity $I(Q)$ for a dilute system of scattering particles can be described by eq 1:

$$I(Q) = I_0 n(\Delta\rho)^2 V^2 P(Q) + I_b \quad (1)$$

where I_0 is an instrument constant, n, the number density of the particles, $\Delta\rho$, the difference in electron density between particles and solvent (contrast), V, the volume of the particles, I_b, the flat background intensity, and $P(Q)$, the particle form factor (*31*). Q is the momentum transfer given by $Q = (4\pi/\lambda)\sin(\theta/2)$, where λ is the X-ray wavelength and θ is the scattering angle.

Scattering curves with no oscillations, but with a power law of −1 in the low Q region, were interpreted using a modified Guinier analysis for rod-like particles (fibers) by plotting $\ln[QI(Q)]$ versus Q^2. From the slope of a fit to a linear Q^2 region at $0.4 < Q_{max}R_c < 1.0$ in the modified Guinier plot the cross-sectional radius of gyration of the fiber, R_c (corresponding radius $R = \sqrt{2}R_c$), can be derived using $R_c^2 = -2 \times$ slope. Scattering data exhibiting a power law of −2 in the lower Q are interpreted using a modified Guinier analysis for sheet-like particles by plotting $\ln[Q^2I(Q)]$ versus Q^2. The slope from a fit to the linear Q^2 region at $QR_t < 0.85$ was used to determine the thickness factor of the sheet, R_t (corresponding thickness $T = (12)^{1/2}R_t$), using $R_t^2 = -$slope.

Scattering curves with oscillations were fit to a hollow circular cylinder (nanotube) model by substituting for $P(Q)$ in eq 1 with the following form factor expression:

$$P(Q) = \int_0^1 \left(\frac{1}{1-(R_2/R_1)^2}\right)^2 \left[\frac{2J_1(QR_1(1-x^2)^{0.5})}{QR_1(1-x^2)^{0.5}} - (R_2/R_1)^2 \frac{2J_1(QR_2(1-x^2)^{0.5})}{QR_2(1-x^2)^{0.5}}\right]^2 \left(\frac{\sin(QLx/2)}{QLx/2}\right)^2 dx \quad (2)$$

where R_1 is the outer radius, R_2, the inner radius, L, the cylinder length, and $J_1(x)$, the Bessel function of the first

order. Although the peak positions and amplitudes agree well between the measured SAXS data and the fits using eq 2, they do not match very well at the minima due to factors such as instrument resolution, presence of smaller aggregates under equilibrium, roughness along the surfaces of the nanotubes, and orientation disorder. We like to point out that the slight disagreement in the amplitudes at the minima will not alter the precision of the structural parameters and conclusions.

Wide Angle X-ray Scattering (WAXS). Powder samples in 1.5 mm diameter quartz capillary tubes were measured at the APS facility using 18 keV X-rays and a sample-to-detector distance of 0.4 m. From the diffraction peaks the repeat distance $d = (2\pi/Q)$ was derived. Intense, sharp, and narrow reflections imply high degree of repetition order while the weaker and broad peaks indicate smaller crystallite size with fewer repetitions or the presence of disorder in the crystallinity.

Isotope-Edited Flourier Transform Infrared Spectroscopy (IE-FTIR). A 500 μL solution of mature tubes or fibers was spun down at 16100*g* for 30 min, and the pellet was frozen at −80 °C and lyophilized. The lyophilized sample was mixed with dehydrated KBr crystals at a ratio of 1:10 (w/w), pressed into a KBr/peptide pellet, and analyzed on a MAGNA-IR 560, ESP instrument operated at 2 cm^{-1} resolution.

Molecular Modeling. Six copies of the seven residue Ac-KLVFFAE-NH_2 peptide were combined twice graphically in Maestro v8.0 (Schrodinger) (*33*) to produce two versions of the six-strand antiparallel β-sheet with full hydrogen bonding as depicted in Scheme 1. The strands were organized either as in-register β-sheets corresponding to fibers or as one-residue-shifted nanotubes. Five copies of the identical sheets were then stacked atop one another to provide five homogeneous laminates. To prepare for subsequent molecular dynamics simulations, the laminates were relieved of unfavorable torsions and steric contacts by energy minimization using the Truncated Newton Conjugate Gradient method and the GBSA/Water continuum solvation model. The relaxed peptide laminates were then enclosed in a truncated octahedral box and surrounded by 30000−60000 SPC water molecules in GROMACS v3.3. For peptides with positive charges, chloride ions were added to make the system neutral. The systems were prepared for MD simulations by performing initial energy minimizations on the aggregates for 10 ps using a steepest descent algorithm followed by solvent equilibration for 20 ps. Unrestrained MD was subsequently carried out for 2 ns at 300 K with a 2 fs time step using the OPLS 2005 force field. The resulting trajectories were viewed with VMD, and rmsd plots were generated using the xmgrace routine in GROMACS. Lipophilic potentials were mapped onto Connolly surfaces generated in the MOLCAD surface viewer with sphere radius of 1.4 Å in SYBYL 7.2 (*34*).

RESULTS

Assembly Morphology. Conditions for the homogeneous assembly of Aβ(16−22), Ac-KLVFFAE-NH_2, into fibers and nanotubes have been described (*31, 32*), and here two conditions are used. When the peptide was dissolved in 40% acetonitrile/water with 0.1% TFA, where both the K16 and E22 side chains are predicted to be protonated and maintain a single positive charge at the N-terminus (acidic condition), the peptide assembles into homogeneous nanotubes. Under the same conditions but containing 0.1 mM NaOH instead of TFA to ionize the Glu side chain (neutral conditions), Aβ(16−22) is expected to carry a positive charge at the N-terminus and a negative charge at the C-terminus. Under these conditions the peptide assembles as homogeneous fibers (*32*). The two morphologies are reversible and interconvert with changes in the assembly conditions, but probably through disassembly as they contain a shift in peptide strand registry (*32*): antiparallel in-register for fibers and antiparallel one residue shifted for nanotubes. It has been suggested that the stability of the pairwise K-E salt bridge contributes to the registry of the fibers and is weakened under the more acidic conditions (*32*).

The contribution of cross-strand pairing complementarity to sheet registry was further evaluated by replacing the only β-branched residue V18 in Aβ(16−22) with a series of amino acids that varied in side chain steric demand. For example, when the 18 position differed by no more than a single CH_2 from valine, e.g., Abu, Leu, norL, and norV, only fibers formed under the acidic conditions (Figure 1). However, the β-branched amino acids Ile and terL directed nanotube assembly, and the most sterically demanding terL congener directed nanotube assembly even under neutral conditions (Figure S1, Supporting Information).

The fiber and nanotube morphologies are readily differentiated in solution by the pronounced oscillations that originate from the differential X-ray reflections of the inner and outer walls of the hollow nanotubes (*31*). In contrast, fibers exhibit a Q^{-1} power law in the low Q region that can be analyzed by a modified Guinier fit with a rod-like or sheet-like form factor. As shown in Figure 2, the fibers have similar diameters, ranging from 8 to 16 nm (Table S1, Supporting Information), or about 3−6 times smaller than the 52 ± 8 nm nanotubes (shell thickness ~4 nm) of V18I and V18terL congeners. The V18terL peptide forms nanotubes that maintain identical cross-sectional area under both neutral and acidic conditions (Figure 2f), and the attenuated amplitude in neutral conditions is consistent with a lower nanotube concentration. Wide-angle X-ray scattering (WAXS) confirmed the characteristic cross-β amyloid pattern (Figure 3 and Table S1, Supporting Information). The 4.7 Å reflection is sharp and strong for all the assemblies, whereas the 10 Å band is specifically characteristic of the nanotubes (Figure 3a) and consistent with a larger number of laminates for these structures (*31, 32, 35*).

Strand Registry. To better visualize the impact of a one-residue shift in β-sheet registry on each face of the β-sheet, they are color coded in Figure 4c. The side chains of K, V, F(20), and E (green bar) alternate with the side chains L, F(19), and A (purple bar) along each face of the register-shifted nanotube β-sheets. In contrast, the in-register sheets isolate K-V-F(20)-E side chains and L-F(19)-A side chains to opposite faces, giving polar and nonpolar β-sheet surfaces.

Strand registry of the antiparallel β-sheets of Aβ(16−22) fibers (*36*) and nanotubes (*32*) displays a range of spectroscopic signatures. Within these Aβ(16−22) congeners, the characteristic β-sheet amide I infrared stretch centered at 1627 cm^{-1} and the higher energy but weaker shoulder at 1694 cm^{-1} proved to be most diagnostic of antiparallel sheets (*32, 37, 38*), independent of strand registry (Figure

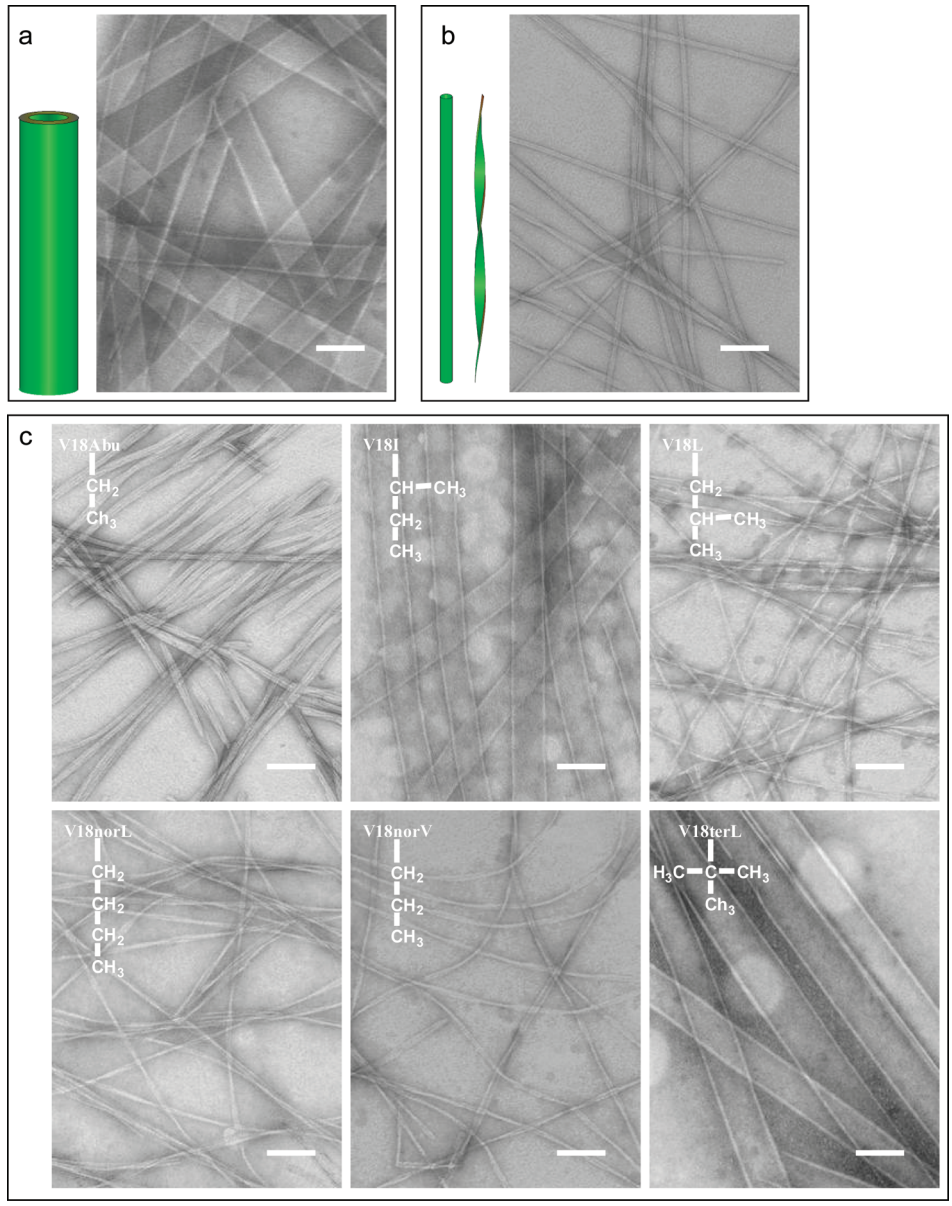

FIGURE 1: TEM of self-assembled structures: (a) Aβ(16−22) nanotubes assembled under acidic conditions, (b) Aβ(16−22) fibers assembled under neutral conditions, and (c) nanotubes or fibers formed by Aβ(16−22) V18 congeners under acidic conditions; scale = 100 nm. Inset: The side chain structure of the residue substituted at the 18 position.

S2, Supporting Information). In addition, isotope-edited FTIR (IE-FTIR) reports on β-sheet strand registry (*39*−*43*) because a β-sheet sequence containing a single ^{13}C carbonyl substitution splits the amide I band into distinct transitions corresponding to the ^{12}C and ^{13}C components at higher and lower energy, respectively. This splitting arises from the mass-dependent vibrational frequency that limits coupling between the ^{12}C and ^{13}C carbonyls along the sheet (*32, 39*−*43*). When ^{13}C carbonyls are aligned and positioned closely within adjacent sheets, transition dipole coupling (TDC) contributes significantly to both the stretching frequency and band separation. For example, Aβ(16−22) nanotubes contain one-residue-shifted antiparallel β-sheets where the carbonyls of F19 are aligned along the center of the β-sheet and the band splitting is 42 cm^{-1} (Figure 4b, carbonyl in red). In contrast, the fibers display in-register antiparallel β-sheets where the F19 carbonyls are cross-aligned and the band splitting is 29 cm^{-1} (Figure 4e).

Under acidic conditions, both V18I and V18terL nanotubes have ^{12}C/^{13}C band splits of 40 and 42 cm^{-1}, respectively, similar to the 42 cm^{-1} for the Aβ(16−22) nanotubes (Figure 4a and Table S2, Supporting Information). The non-β-branched congener fibers have ^{12}C and ^{13}C band splits in a range of 27−32 cm^{-1}; V18Abu (27 cm^{-1}), V18L (32 cm^{-1}), V18norL (29 cm^{-1}), and V18norV (28 cm^{-1}) (Figure 4a and Table S2, Supporting Information), reflecting the Aβ(16−22) fiber's value of 29 cm^{-1}. The V18terL nanotubes under neutral conditions also have a ^{12}C/^{13}C band split of 42 cm^{-1}, consistent with the one-residue-shifted registry (Figure 4d and Table S2, Supporting Information), whereas all other V18 congeners under neutral assembly conditions have ^{12}C/^{13}C amide I bands separated by 24−32 cm^{-1}, assigned as in-register backbone arrays. Therefore, within the V18 congener β-sheets, one-residue-shifted strands are present in the nanotube morphologies and in-register assemblies are present in fibers, just as in native Aβ(16−22).

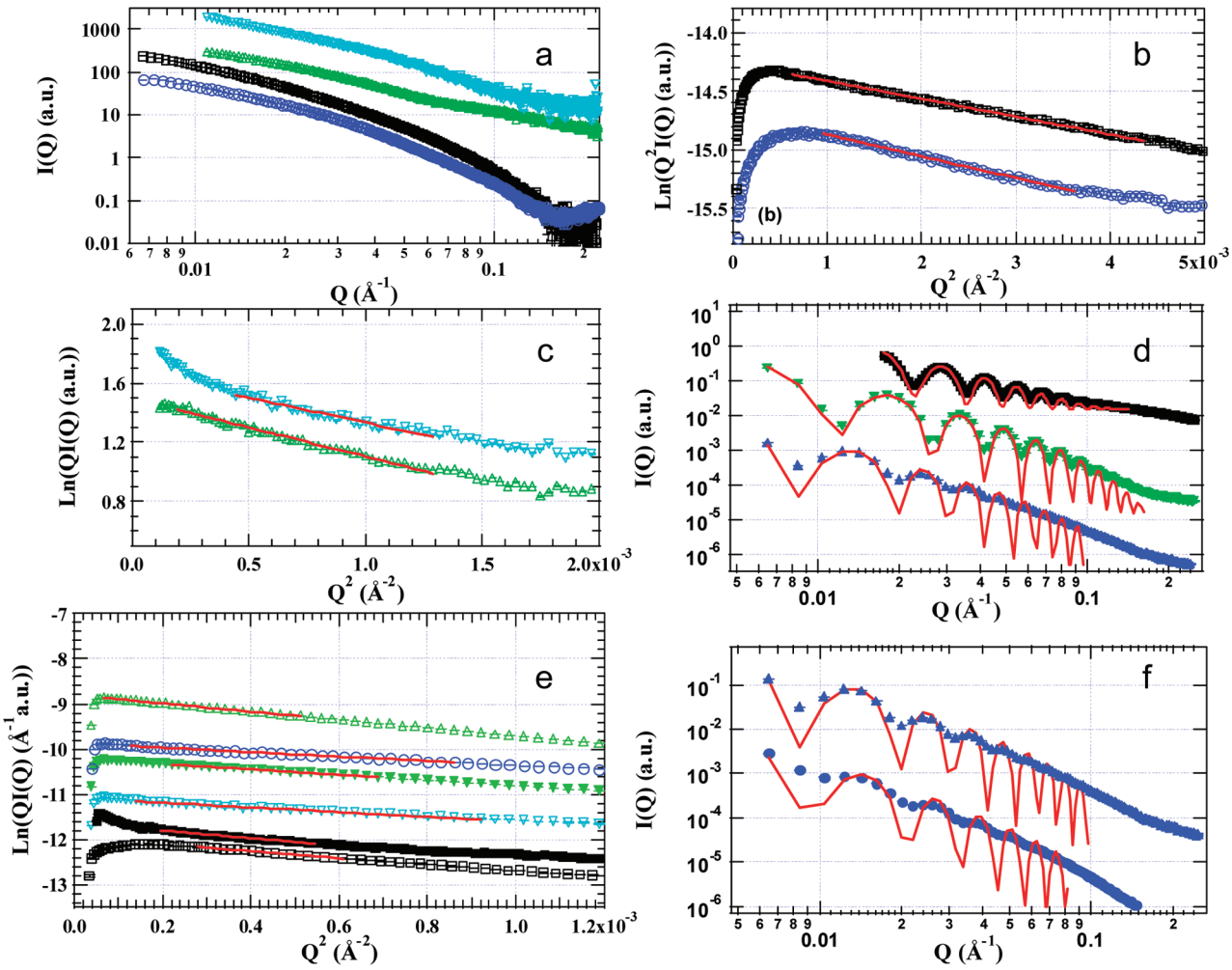

FIGURE 2: SAXS of V18 congeners. (a) SAXS of fibers assembled under acidic conditions: V18Abu (□, black), V18L (Δ, green), V18norL (∇, cyan), and V18norV (○, blue). (b) Modified Guinier analysis of fibers assembled under acidic conditions with sheet-like forms (fit in red): V18Abu (□, black) and V18norV (○, blue). (c) Modified Guinier analysis of fibers assembled under acidic conditions with rod-like forms (fit in red): V18L (△, green) and V18norL (▽, cyan). (d) SAXS scattering of tubes under acidic conditions and their shell core circular cylinder fitting (in red): Aβ(16−22) (■, black), V18I (▼, green), and V18terL (▲, blue). (e) Modified Guinier analysis of fibers assembled under neutral conditions with rod-like forms (fit in red): Aβ(16−22) (■, black), V18I (▼, green), V18Abu (□, black), V18L (Δ, green), V18norL (▽, cyan), and V18norV (○, blue). (f) SAXS scattering of V18terL tubes and their shell core circular cylinder fitting (in red): formed under acidic (▲, blue) and neutral conditions (●, blue).

Molecular Modeling. To approximate side chain arrangements, the structural features of the six-strand, five-sheet Aβ(16−22) arrays were captured by averaging over the last 20 ps of the trajectories of molecular dynamics (MD) simulations. Lipophilic surfaces were generated in Sybyl for the central β-sheet, namely, the third strand in each of the laminates. Figure 5 displays this averaged property for the top and bottom surfaces of the one-residue-shifted and in-register β-sheets. For the one-residue-shifted sheet, both surfaces appear very similar. In contrast, the in-register β-sheet surfaces differ significantly in their lipophilic characteristics. Furthermore, Lys-Glu cross-strand electrostatic interactions are abundant between adjacent peptides within the in-register β-sheets (Figure S3, Supporting Information), suggesting an important contribution to the in-register β-sheet stability. This feature is absent in the one-residue-shifted sheet models because Lys and Glu in the adjacent strands are positioned on opposite sides of each sheet (Figure 4c and Figure S4, Supporting Information). Hydrogen bonding between the polar Lys and Glu residues is precluded within the β-sheets. Therefore, the modeling predicts the Lys-Glu salt bridges under neutral conditions could indeed contribute substantial electrostatic stabilization to the in-register β-sheet integrity.

Since energetic differences resulting from changing nonpolar amino acid side chains to β-branched ones are assumed to be largely steric, these differences were probed using molecular mechanics. Especially in the absence of explicit solvent, force fields overemphasize electrostatic interaction energies (*44*). On the other hand, they are well parametrized to reproduce steric energies. To minimize the role played by side chain electrostatic interactions that might lead to energetic overstabilization and to estimate the steric contribution of cross-strand pairing to the stability of β-sheet assemblies, the Lys and Glu residues in each peptide strand were replaced with alanine and the relative energies estimated with energy minimization (Table S3, Supporting Information). For each peptide, the central three-strand β-sheets were compared, either in-register or one-residue-shifted antiparallel registry, and the structures minimized with both OPLS 2005 and AMBER 94. When expressed as $\Delta\Delta E$ ($\Delta E_{\text{one-residue-shifted}} - \Delta E_{\text{in-register}}$), the in-register arrangement, which contains

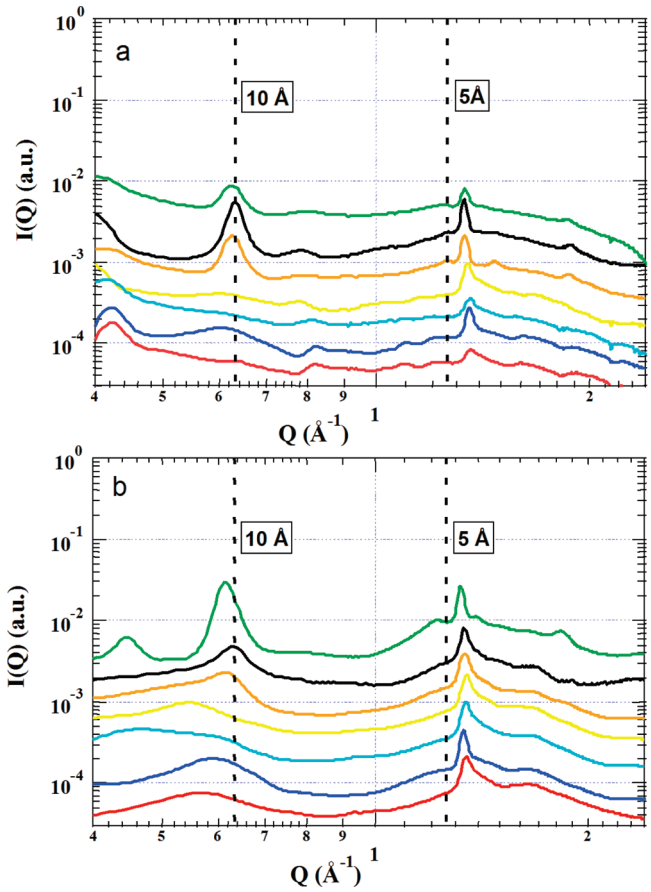

FIGURE 3: Interstand and intersheet WAXS of powders of Aβ(16−22) and V18 congeners, V18terL (green), Aβ(16−22) (black), V18I (orange), V18norV (yellow), V18norL (cyan), V18L (blue), and V18Abu (red) assembled under (a) acidic or (b) neutral conditions.

one additional H-bond, is lower in energy in each case. However, with β-branched residues at 18, the energy difference is reduced significantly (Table S3, Supporting Information), consistent with the β-branched residue at 18 preferring the one-residue-shifted registry. For example, the peptide with the non-β-branched Leu at 18 has the largest absolute $\Delta\Delta E$, about 4 kcal/mol. With the β-branched residue, Val or Ile, the $\Delta\Delta E$s are reduced to 2.5 kcal/mol, and with terL, the $\Delta\Delta E$ is further reduced to 0.5 kcal/mol. These results are consistent with the experimental observation that peptides with β-branched residues at 18 significantly favor a one-residue-shifted registry and support side chain packing along the sheet face as a significant contributor to β-sheet assembly and amyloid nucleation.

To determine the hydrophobic surface burial between non-β-branched and β-branched amino acid side chains within the Aβ(16−22) V18 congeners, their three-strand antiparallel in-register or one-residue-shifted β-sheets were compared (Table S4, Supporting Information). For each peptide, the buried surface area was calculated by subtracting the solvent-accessible surface area (SASA) value in the β-sheet from its corresponding value in the random coil (*14, 45*). The Val, Ile, or Leu congeners did not differ significantly in the mean fraction buried, *f*, which is an intrinsic measurement of the hydrophobicity (*45*). More significantly, the peptides with Leu or Ile at 18 have the same number of atoms, and their difference in buried surface area upon forming the β-sheet is less than 1% in both in-register and one-residue-shifted β-sheets.

DISCUSSION

The assembly of secondary structural elements is of critical importance in protein folding, and both experimental evidence (*46*) and bioinformatic analyses (*11, 12*) have implicated cross-strand pairing as a contributor to β-sheet assembly and stability in globular proteins. However, recent evidence suggests that formation of a single isolated β-sheet might be regulated by hydrophobic surface burial events that dominate other β-sheet propensity measures (*14*). This difference suggests that the early steps in protein misfolding, events that have been debated for many years (*17*−*19*), could be structurally probed in amyloid. Accordingly, we sought to use the simple core segment from the Alzherimer's disease peptide Aβ to investigate early β-sheet nucleation during assembly.

Our modeling results suggest that small energy differences underlie β-sheet peptide registry, and yet these differences can be sufficient to lead to the exclusive formation of a single sheet morphology, manifested as either amyloid nanotubes or fibers in Ac-KLVFFAE-NH_2, Aβ(16−22). The Lys and Glu residues at the N- and C-termini of Aβ(16−22) are positioned as cross-strand pairs that could stabilize antiparallel β-sheets through side chain salt bridges (*11, 12, 14*). Indeed, MD simulations support extended pairwise K-E ladders or networks (*47*) formed along the β-sheet surface that stabilize the in-register antiparallel β-sheets formed in Aβ(16−22) fibers. However, the magnitude of the K-E ladder stabilization is expected to depend on the desolvation penalties and the required loss of side chain entropy (*47*−*49*) that make these assemblies so challenging to model. Nevertheless, the protonation of the Glu side chains in Aβ(16−22) tubes, which should weaken the K-E ladders, results in one-residue-shifted β-sheets, removing one H-bond per strand and placing the K and E residues on opposite faces of each sheet.

This shift in registry may well be driven by another pairwise constraint with V18, shifting the β-branched V18 from cross-strand pairing with F20 to being paired with the smaller A21. Only β-branching at residue 18 shifts the registry, such that residues of the same composition without β-branching only form in-register fibers. When the steric size of V18 is increased to terL, the one-residue-shifted antiparallel β-sheet forms independent of the Lys and Glu side chain protonation states.

While these data make a compelling case for an energetic contribution from cross-strand pairing, several other elements require consideration. First, in the OspA sheet (*14, 45*), hydrophobic surface burial was critical but does not appear to be a major contributor in self-assembly of the Aβ(16−22) V18 congeners. However, as a measure of surface area buired, the "lipophilic" surface area did appear more "complementary" in the one-residue-shifted orientation. As shown in Figure 5, the sheet surfaces show little energetic preference for stacking top-top, top-bottom, or bottom-bottom faces. In contrast, one surface of the in-register β-sheet is markedly more hydrophobic, such that assembly between two bottom surfaces, burying the most hydrophobic surfaces,

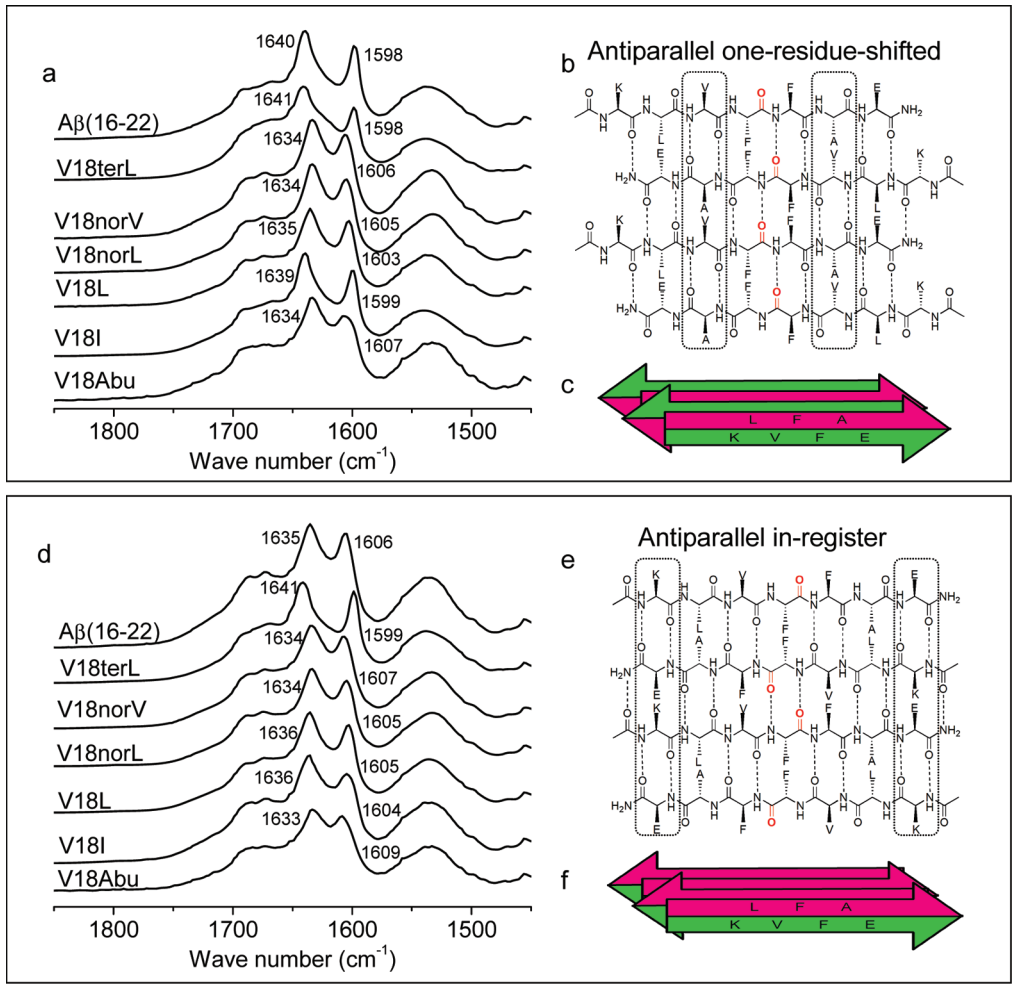

FIGURE 4: IE-FTIR of Aβ(16−22) and V18 congeners: (a) $^{12}C/^{13}C$ amide I absorbance under acidic conditions; (b) antiparallel one-residue-shifted β-sheet of Aβ(16−22) with F19 carbonyl in red; (c) side chain distribution of the antiparallel one-residue-shifted Aβ(16−22) β-sheet, K-V-F(20)-E in green and L-F(19)-A in pink; (d) $^{12}C/^{13}C$ amide I absorbance under neutral conditions; (e) antiparallel in-register β-sheet of Aβ(16−22) with F19 carbonyl in red; (f) side chain distribution of the antiparallel in-register Aβ(16−22) β-sheet, K-V-F(20)-E in green and L-F(19)-A in pink.

might be anticipated. Such differences in lipophilic surface area could impact nucleation and growth of the in-register antiparallel β-sheets of the fiber. However, if the peptides are in the same registry, the inclusion of β-branching at position 18 in Aβ(16−22), or even the addition of a single methyl group to the peptide in the case of terL, has little or no impact on the predicted lipophilicity of these surfaces and should not dictate registry.

A second important consideration of β-branching could be its impact on the peptide backbone. In the repeating antiparallel amyloid assembly, each side chain exists in H-bonding and non-H-bonding positions with the same cross-strand neighbor (Scheme 1), averaging these differences. Initial molecular modeling of Aβ(10−35), however, suggested that the overall planarity of the β-sheet is limited by the length of the H-bonded peptide strand (*50, 51*). Small segments of about six amino acids remained as planar H-bonded segments, but side chain/backbone interactions destabilized longer stretches. Obviously, the one-residue-shifted β-strands in the nanotubes of Aβ(16−22) possess one fewer residue involved in backbone H-bonding; however, MD identified no significant difference in the "flatness" of any of the Aβ(16−22) fiber and nanotube β-sheets, suggesting that such intrastrand interactions are not significant in determining the registry of these short sequences.

These results then highlight backbone registry as a delicate balance between pairwise K-E association and the steric demand at the β-carbon of residue 18. And terL-Ala cross-strand pairing appears to override the favorable K-E ladders even at their strongest electrostatic interaction when both side chains are ionized, underscoring the importance of pairwise associations, both electrostatic and β-branching, in amyloid strand assembly. While such pair correlations are typical of the constraints seen in globular protein folding (*7*−*13*), they appear to be of secondary importance for the thermodynamic stability of the exposed β-sheet of OspA. Rather, buried nonpolar surface area has emerged as most critical when both faces of the sheet are solvent exposed (*14*), consistent with desolvation providing the critical energetic constraint for protein folding (*52*−*55*). Further, recent work on solvent effects on insulin self-assembly further stresses the critical impact of hydration on the amyloid nuclei (*56*−*58*). Therefore, current amyloid assembly models, which score for single solvent-exposed sheets (*26*−*30*) where secondary structure and strand registry are set in the initial nucleus, by this analysis, should be controlled by nonpolar surface area burial.

It may be that in the larger OspA protein cross-strand pair interactions in the single connecting sheet are dominated by the folding of the larger protein domains at either end of the

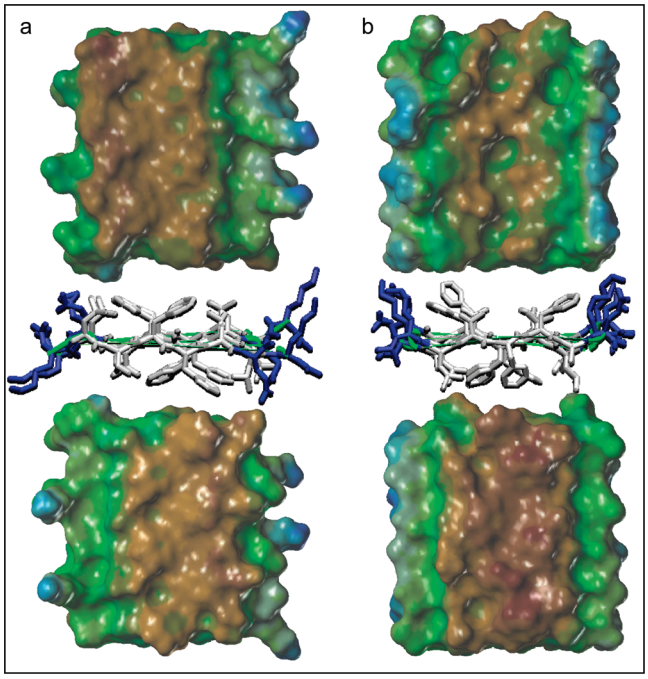

FIGURE 5: Surface lipophilicity of (a) Aβ(16−22) antiparallel one-residue-shifted β-sheet and (b) Aβ(16−22) antiparallel in-register β-sheet. Color scale of lipophilicity: brown, more hydrophbobic, to blue, more hydrophilic. Color of four-strand β-sheet: backbone is in green, Lys and Glu are in blue, and hydrophobic residues are in white.

sheet. Alternatively, the shorter Aβ(16−22) peptide may be desolvated early through some accumulating hydrophobic collapse, much like globular proteins, allowing the intrinsic β-sequence and pair correlations to regulate secondary assembly. The nature of such early desolvation events could be accounted for by early particle assemblies (*59, 60*), but the nature of these assemblies and their contribution to amyloid nucleation remains unclear. Accordingly, future efforts must focus on factors that contribute to sheet desolvation during the early stages of amyloid assembly. Resolving these differences could well open new strategies for controlling amyloid assembly and the regulation of misfolding diseases.

ACKNOWLEDGMENT

We gratefully acknowledge the support by DOE ER15377, NSF-CHE 0404677, and NSF-CHE 0739189 and the excellent assistance of Soenke Seifert in the X-ray scattering experiments at the Advanced Photon Source at the Argonne National Laboratory funded by the DOE, BES, under contract DE-AC02-06CH11357 to the U. Chicago Argonne, LLC. We further acknowledge the use of the Apkarian Electron Microscopy Facility and the Center for the Analysis of Supramolecular Self-assemblies for Atomic Force Microscopy at Emory University.

SUPPORTING INFORMATION AVAILABLE

Table S1, structural parameters from the SAXS of solutions and WAXS of powders of fibers and nanotubes formed by Aβ(16−22) and its congeners under both neutral and acidic conditions; Table S2, ^{12}C and ^{13}C amide I band shifts in IE-FTIR of fibers and nanotubes formed by Aβ(16−22) and its V18 cogeners under both neutral and acidic conditions; Table S3, energy difference between in-register and one-residue-shifted-register of Aβ(16−22) and its V18 congeners; Table S4, buried surface area of Aβ(16−22) and its V18 congeners; Figure S1, TEM of fibers and tubes formed by Aβ(16−22) V18 congeners under neutral conditions; Figure S2, FTIR amide I band of Aβ(16−22) and all V18 congener self-assembled structures; Figure S3, side chain distance variation of Lys-Glu pairs (ladders) in the in-register Aβ(16−22) β-sheet over a 2 ns MD simulation; Figure S4, side chain distance variation of Lys and Glu from two one-residue-shifted Aβ(16−22) β-sheets over the 2 ns MD simulation. This material is available free of charge via the Internet at http://pubs.acs.org.

REFERENCES

1. Wojcik, J., Altman, K. H., and Scheraga, H. A. (1990) Helix-coil stability constants for the naturally occurring amino acids in water. XXIII. Proline parameters from random poly(hydroxybutylglutamineco-L-proline). *Biopolymers 30*, 121–134.
2. Lyu, P. C., Liff, M. I., Marky, L. A., and Kallenbach, N. R. (1990) Side chain contributions to the stability of α-helical structure in peptides. *Science 250*, 669–673.
3. O'Neil, K. T., and DeGrado, W. F. (1990) A thermodynamic scale for the helix forming tendencies of the commonly occurring amino acids. *Science 250*, 646–651.
4. Padmanabhan, S., Marqusee, S., Ridgeway, T., Laue, T. M., and Baldwin, R. L. (1990) Relative helix-forming tendencies of nonpolar amino acids. *Nature 344*, 268–270.
5. Horovitz, A., Matthews, J. M., and Fersht, A. R. (1992) α-Helix stability in proteins: II. Factors that influence stability at an internal position. *J. Mol. Biol. 227*, 560–568.
6. Blaber, M., Zhang, X. J., and Matthews, B. W. (1993) Structural basis of amino acid α-helix propensity. *Science 260*, 1637–1640.
7. Chou, P. Y., and Fasman, G. D. (1974) Conformational parameters for amino acids in helical, β-sheet, and random coil regions calculated from proteins. *Biochemistry 13*, 211–222.
8. Minor, D. L., Jr., and Kim, P. S. (1994) Measurement of the β-sheet-forming propensities of amino acids. *Nature 367*, 660–663.
9. Kim, C. A., and Berg, J. M. (1993) Thermodynamic β-sheet propensities measured using a zinc-finger host peptide. *Nature 362*, 267–270.
10. Minor, D. L., Jr., and Kim, P. S. (1994) Context is a major determinant of β-sheet propensity. *Nature 371*, 264–267.
11. Wouters, M. A., and Curmi, P. M. G. (1995) An analysis of side chain interactions and pair correlations within antiparallel β-sheets: the difference between backbone hydrogen-bonded and non-hydrogen-bonded residue pairs. *Proteins: Struct., Funct., Genet. 22*, 119–131.
12. Hutchinson, E. G., Sessions, R. B., Thornton, J. M., and Woolfson, D. N. (1998) Determinants of strand register in antiparallel β-sheet of protein. *Protein Sci. 7*, 2287–2300.
13. Zaremba, S. M., and Gregoret, L. M. (1999) Context-dependence of amino acid residue pairing in antiparallel β-sheet. *J. Mol. Biol. 291*, 463–479.
14. Yan, S., Gawlak, G., Makabe, K., Tereshko, V., Koide, A., and Koide, S. (2007) Hydrophobic surface burial is the major stability determinant of a flat, single layer β-sheet. *J. Mol. Biol. 368*, 230–243.
15. Makabe, K., McElheny, D., Tereshko, V., Hilyard, A., Gawlak, G., Yan, S., Koide, A., and Koide, S. (2006) Atomic structures of peptide self-assembly mimics. *Proc. Natl. Acad. Sci. U.S.A. 103*, 17753–17758.
16. Makabe, K., Yan, S., Tereshko, V., Gawlak, G., and Koide, S. (2007) β-Strand flipping and slipping triggered by turn replacement reveal the opportunistic nature of β-strand pairing. *J. Am. Chem. Soc. 129*, 14661–14669.
17. Harper, J. D., Peter, T., and Lansbury, J. (1997) Models of amyloid seeding in Alzheimer's disease and scrapie: mechanistic truths and physiological consequences of the time-dependent solubility of amyloid proteins. *Annu. Rev. Biochem. 66*, 385–407.
18. Westermark, P. (2005) Aspects on human amyloid forms and their fibril polypeptides. *FEBS J. 272*, 5942–5949.

19. Wetzel, R. (2006) Kinetics and thermodynamics of amyloid fibril assembly. *Acc. Chem. Res. 39*, 671–679.
20. Blake, C., and Serpell, L. (1996) Synchrotron X-ray studies suggest that the core of the transthyretin amyloid fibril is a continuous β-sheet helix. *Structure 4*, 989–998.
21. Sunde, M., Serpell, L. C., Bartlam, M., Fraser, P. E., Pepys, M. B., and Blake, C. C. F. (1997) Common core structure of amyloid fibers by synchrotron X-ray diffraction. *J. Mol. Biol. 273*, 729–739.
22. Sikorski, P., Atkins, E. D. T., and Serpell, L. C. (2003) Structure and texture of fibrous crystals formed by Alzheimer's Aβ(11−25) peptide fragment. *Structure 11*, 915–926.
23. Dobson, C. M. (2003) Protein folding and misfolding. *Nature 426*, 884–890.
24. Uversky, V. N., and Finka, A. L. (2004) Conformational constraints for amyloid fibrillation: the importance of being unfolded. *Biochim. Biophys. Acta 1698*, 131–153.
25. Dobson, C. M. (2004) Experimental investigation of protein folding and misfolding. *Methods 34*, 4–14.
26. Nguyen, H. D., and Hall, C. K. (2004) Molecular dynamics simulations of spontaneous fibril formation by random-coil peptides. *Proc. Natl. Acad. Sci. U.S.A. 101*, 16180–16185.
27. Urbanc, B., Cruz, L., Ding, F., Sammond, D., Khare, S., Buldyrev, S. V., Stanley, H. E., and Dokholyany, N. V. (2004) Molecular dynamics simulation of amyloid β dimer formation. *Biophys. J. 87*, 2310–2321.
28. Hwang, W., Zhang, S., Kamm, R. D., and Karplus, M. (2004) Kinetic control of dimer structure formation in amyloid fibrillogenesis. *Proc. Natl. Acad. Sci. U.S.A. 101*, 12916–12921.
29. Ikebe, J., Kamiya, N., Ito, J.-I., Shindo, H., and Higo, J. (2007) Simulation study on the disordered state of an Alzheimer's β amyloid peptide Aβ(12−36) in water consisting of random-structural, β-structural, and helical clusters. *Protein Sci. 16*, 1596–1608.
30. Jang, S., and Shin, S. (2008) Computational study on the structural diversity of amyloid beta peptide (Aβ10−35) oligomers. *J. Phys. Chem. B 112*, 3479–3484.
31. Lu, K., Jacob, J., Thiyagarajan, P., Conticello, V. P., and Lynn, D. (2003) Exploiting amyloid fibril lamination for nanotube self-assembly. *J. Am. Chem. Soc. 125*, 6391–6393.
32. Mehta, A. K., Lu, K., Childers, W. S., Liang, Y., Dublin, S., Dong, J., Snyder, J. P., Skanthakumar, S., Thiyagarajan, P., and Lynn, D. G. (2008) Facial symmetry in self-assembly. *J. Am. Chem. Soc. 130*, 9829−9835.
33. Spoel, D. v. d., Lindahl, E., Hess, B., Buuren, A. R. v., Apol, E., Meulenhoff, P. J., Tieleman, D. P., Sijbers, A. L. T. M., Feenstra, K. A., Drunen, R. v., and Berendsen, H. J. C. (2005) Gromacs User Manual version 3.3, www.gromacs.org.
34. SYBYL 7.3, Tripos International, 1699 South Hanley Rd., St. Louis, MO 63144.
35. Dong, J., Lu, K., Lakdawala, A., Mehta, A. K., and Lynn, D. (2006) Controlling amyloid growth in multiple dimensions. *Amyloid 13*, 206–215.
36. Antzutkin, O. N., Leapman, R. D., Balbach, J. J., and Tycko, R. (2002) Supramolecular structural constraints on Alzheimer's β-amyloid fibers from electron microscopy and solid-state nuclear magnetic resonance. *Biochemistry 41*, 15436–15450.
37. Elliott, A., Ambrose, E. J., and Robinson, C. (1950) Chain configurations in natured and denatured insulin: evidence from infrared spectra. *Nature 166*, 194.
38. Halverson, K. J., Sucholeiki, I., Ashburn, T. T., and Lansbury, P. T., Jr. (1991) Location of β-sheet-forming sequences in amyloid proteins by FTIR. *J. Am. Chem. Soc. 113*, 6701–6703.
39. Kubelka, J., and Keiderling, T. A. (2001) The anomalous infrared amide I intensity distribution in ^{13}C isotopically labeled peptide β-sheets comes from extended, multiple-stranded structures, An ab initio study. *J. Am. Chem. Soc. 123*, 6142–6150.
40. Hiramatsu, H., and Kitagawa, T. (2005) FTIR approaches on amyloid fibril structure. *Biochim. Biophys. Acta 1753*, 100–107.
41. Paul, C., and Axelsen, P. H. (2005) β-sheet structure in amyloid β fibers and vibrational dipolar coupling. *J. Am. Chem. Soc. 127*, 5754–5755.
42. Petty, S. A., and Decatur, S. M. (2005) Experimental evidence for the reorganization of β-strands within aggregates of the Aβ(16−22) peptide. *J. Am. Chem. Soc. 127*, 13488–13489.
43. Decatur, S. M. (2006) Elucidation of residue-level structure and dynamics of polypeptides via isotope-edited infrared spectroscopy. *Acc. Chem. Res. 39*, 169–175.
44. Lakdawala, A., Wang, M., Nevins, N., Liotta, D., Rusinska-Roszak, D., Lozynski, M., and Snyder, J. P. (2001) Calculated conformer energies for organic molecules with multiple polar functionalities are method dependent: Taxol (case study). *BMC Chem. Biol. 1*, 2.
45. Lesser, G. J., and Rose, G. D. (1990) Hydrophobicity of amino acid subgroups in proteins. *Proteins: Struct., Funct., Genet. 8*, 6–13.
46. Smith, C. K., and Regan, L. (1995) Guidelines for protein design: the energetics of β sheet side chain interactions. *Science 270*, 980–982.
47. Kumar, S., and Nussinov, R. (2002) Close-range electrostatic interactions in proteins. *ChemBioChem 3*, 604–617.
48. Hendsch, Z. S., and Tidor, B. (1994) Do salt bridges stabilize proteins? A continuum electrostatic analysis. *Protein Sci. 3*, 211–226.
49. Honig, B., and Nicholis, A. (1995) Classical electrostatics in biology and chemistry. *Science 268*, 1144–1149.
50. Lakdawala, A. S., Morgan, D. M., Liotta, D. C., Lynn, D. G., and Snyder, J. P. (2002) Dynamics and fluidity of amyloid fibers: a model of fibrous protein aggregates. *J. Am. Chem. Soc. 124*, 15150–15151.
51. Morgan, D. M., Dong, J., Jacob, J., Lu, K., Apkarian, R. P., Thiyagarajan, P., and Lynn, D. G. (2002) Metal switch for amyloid formation: insight into the structure of the nucleus. *J. Am. Chem. Soc. 124*, 12644–12645.
52. Fernandez, A., Kardosb, J., and Gotob, Y. (2003) Protein folding: could hydrophobic collapse be coupled with hydrogen-bond formation? *FEBS J. 536*, 187–192.
53. Avbelj, F., and Baldwin, R. L. (2002) Role of backbone solvation in determining thermodynamic β propensities of the amino acids. *Proc. Natl. Acad. Sci. U.S.A. 99*, 1309–1313.
54. Rodriguez-Larrea, D., Ibarra-Molero, B., and Sanchez-Ruiz, J. M. (2006) Energetic and structural consequences of desolvation/solvation barriers to protein folding/unfolding assessed from experimental unfolding rates. *Biophys. J. Biophys. Lett.,* , L48−L50.
55. Fernandez, A., Sosnick, T. R., and Colubri, A. (2002) Dynamics of hydrogen bond desolvation in protein folding. *J. Mol. Biol. 321*, 659–675.
56. Dzwolak, W., Ravindrab, R., and Winter, R. (2004) Hydration and structure—the two sides of the insulin aggregation process. *Phys. Chem. Chem. Phys. 6*, 1938–1943.
57. Dzwolak, W., Grudzielanek, S., Smirnovas, V., Ravindra, R., Nicolini, C., Jansen, R., Loksztejn, A., Porowski, S., and Winter, R. (2005) Ethanol-perturbed amyloidogenic self-assembly of insulin: Looking for origins of amyloid strains. *Biochemistry 44*, 8948–8958.
58. Smirnovas, V., Winter, R., Funck, T., and Dzwolak, W. (2006) Protein amyloidogenesis in the context of volume fluctuations: A case study on insulin. *ChemPhysChem 7*, 1046–1049.
59. Necula, M., Kayed, R., Milton, S., and Glabe, C. G. (2007) Small molecule inhibitors of aggregation indicate that amyloid beta oligomerization and fibrillization pathways are independent and distinct. *J. Biol. Chem. 282*, 10311–10324.
60. Kayed, R., Head, E., Sarsoza, F., Necula, M., Margol, L., Wu, J., Breydo, L., Thompson, J. L., Rasool, S., Gurlo, T., Butler, P., and Glabe, C. G. (2007) Fibril specific, conformation dependent antibodies recognize a generic epitope common to amyloid fibers and fibrillar oligomers that is distinct from prefibrillar oligomers. *Mol. Neurodegeneration 2*, 1–11.

BI801081C